Journal of
Nanoscience and Nanotechnology
Vol. 8, 1–10, 2007

Effects of Ampholyte Dissociation Constants on Protein Separation in On-Chip Isoelectric Focusing

Jaesool Shim[1], Prashanta Dutta[1,*], and Cornelius F. Ivory[2]

[1] *School of Mechanical and Materials Engineering, Washington State University, Pullman, WA 99164-2920, USA*
[2] *School of Chemical Engineering and Bioengineering, Washington State University, Pullman, WA 99164-2710, USA*

Numerical simulations are presented for ampholyte-based isoelectric focusing in 2D microgeometries. In this study, model proteins are focused in the presence of 25 biprotic ampholytes under an applied electric field. Each protein is considered as a simple polypeptide having ten charge states, while the biprotic ampholytes are selected to generate a shallow pH range of 6 to 9. Straight and contraction-expansion microchannels are considered here, and a nominal electric field of 300 V/cm is maintained for separation of proteins. Six distinct values of ΔpKs between 1 and 3.5 are investigated for ampholytes to form pH profiles in a 1 cm long microchannel. Simulation results show that relatively larger values of $\Delta pK (\Delta pK > 3)$ are required to form stepless pH profiles in the system. The peak heights and differential resolutions of focused proteins are much higher for lower values of ΔpK for which a stepped pH profile is evident. For each protein, the time it takes for the two edges of a peak to merge increases linearly with ΔpK, while the focusing time goes up exponentially with increasing ΔpK. Both merging and focusing times of protein are higher for contraction-expansion microchannel than those of straight microchannel. For a particular value of ΔpK, the contracted "Zoom" region of contraction-expansion channel is able to form more tightly focused bands than the expanded region.

Keywords: Isoelectric Focusing, pH Gradient, Biprotic Ampholytes, Protein, Microchannel.

RESEARCH ARTICLE

1. INTRODUCTION

Isoelectric focusing (IEF) is widely used as a separation technique in a variety of applications including proteomics, drug discovery, diagnostics and routine laboratory analysis of commercial proteins due to its high resolving power. In IEF, charged macromolecules are separated and/or focused in a pH gradient under the influence of an electric field. Generally carrier ampholytes, a mixture of low molecular weight amphoteric molecules, are used to form a stable pH gradient along the channel axis.[1,2]

IEF, an equilibrium gradient method,[3] can concentrate low abundance proteins up to about 10 mgs/ml and resharpen peaks if they have been dispersed for any reason. This ability to self-sharpen allows the designer to consider using compact runs of densely-spaced serpentine channels without requiring hyperturns to minimize dispersion. Other important advantages of IEF are that it is performed in a fixed channel length and that, to a first approximation, resolution depends on the potential difference between the electrodes rather than on the channel length.

Today IEF is routinely used by researchers in both bench- and micro-scale devices. Due to its high importance to the field of bio-separation, a number of research groups have developed one-dimensional analytical and numerical models to elucidate the behavior of IEF in capillaries and micro-chips.[4–9] A generalized mathematical model of IEF and other electrophoretic techniques was first introduced by Palusinski et al.[10] for steady state processes. Later, Bier et al.[11] extended this model to transient problems. In a research monograph, Mosher et al.[6] reported their method of handling weak and strong acids and bases, ampholytes, and proteins for ampholyte-based pH gradient IEF. For IEF in the presence of many ampholytes, Mao et al.[5] simulated the transient dynamics of capillary isoelectric focusing (cIEF) using a 1D computational geometry with 150 ampholytes to cover the broad pH range ~3–10. On the other hand, Arnaud et al.[7] simulated off-gel buffering, i.e., neutralization of ampholytes in a solution before penetrating the gel, using the finite element method (FEM). Later, Gas et al. simulated isoelectric focusing in free solution with a correction for ionic mobilities[12,13] using Onsager-Fuoss theory.[14] All the above works modeled and/or simulated one-dimensional computational geometry such as

*Author to whom correspondence should be addressed.

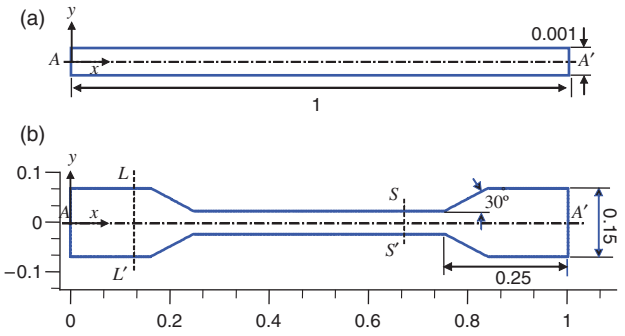

Fig. 1. Schematic of 2D microchannel geometries used in the numerical simulation of ampholyte-based IEF. (a) Straight microchannel and (b) contraction-expansion microchannel. All dimensions are in [cm]. In the contraction-expansion microchannel, the widths at the expanded (L − L′) and throat (S − S′) regions are 1.5 mm and 0.5 mm, respectively.

capillary tube. Recently, Shim et al.[15] presented a mathematical and computational model for ampholyte-based IEF in 2D microgeometries; the effects of 2D microgeometries on protein separation are identified.

In experimental and theoretical IEF work, a linear pH profile along the channel is assumed to estimate the position of focused target components. However, the formation of a linear pH profile depends on a number of parameters such as electric field, pH range, channel geometry, the number of carrier ampholytes in solution, dissociation constants of ampholytes, etc. For a particular channel geometry, electric field, and ampholyte number, the shape of the pH profile depends primarily on the quality of the amphoteric molecules. In electrophoretic process, ampholytes are generally characterized by their dissociation constants (pKs). Hence, in this study, simulation results are presented for various values of the ampholytic ΔpKs to demonstrate the effects of dissociation constants on the formation of the pH profile. Like our previous study,[15] 2D straight and contraction-expansion microchannels (Fig. 1) are chosen as sample geometries to demonstrate the effect of channel width in IEF separation. The separation resolution, peak height, and resulting bandwidth are presented for different values of ΔpKs in both straight and contraction-expansion microchannels to identify the optimum dissociation constants of biprotic ampholytes for each microchannel.

2. MATHEMATICAL MODEL

The mathematical model for multidimensional IEF is presented in our earlier publication.[15] In this section, we briefly review the governing equations used in the numerical model. Ampholyte-based IEF takes place in a soup of partially-ionized solutes whose charge characteristics are determined by a set of dissociation reactions. In IEF, one can treat each component, C_i, as being composed of a set of $J_i + 1$ species, S_{ij}, which are summed over j to recover each of the i components in the system with a total of J_i dissociable groups., i.e.,

$$C_i = \sum_{j=1}^{J_i+1} S_{ij} \tag{1}$$

This relation allows us to treat all weak acids and bases, ampholytes, proteins and even water, which dissociates into hydronium and hydroxide ions, as being mathematically equivalent. Therefore, the mean charge, $\langle z_i \rangle$, of a component, C_i, can be defined as follows,

$$\langle z_i \rangle C_i = \sum_{j=1}^{J_i+1} z_{ij} S_{ij} \tag{2}$$

where z_{ij} is the charge of jth specie of the ith component in the system.

The mass conservation equation for each component (C_i) is obtained by summing the conservation equations for the J_{i+1} species to yield[15]

$$\frac{\partial}{\partial t} C_i - \nabla \cdot (D_i \nabla C_i) + \nabla \cdot (\vec{U} C_i) + \nabla \cdot (\omega_i \vec{E}) \sum_{j=1}^{J_{i+1}} (z_{ij} S_{ij}) = 0 \tag{3}$$

where $\vec{E}$ is the electric field, D_i and ω_i are the diffusion coefficient and absolute mobility of component i, respectively. Then using Eq. (2), we obtain

$$\frac{\partial}{\partial t} C_i + \nabla \cdot ((\vec{U} + \langle z_i \rangle \omega_i \vec{E}) C_i - D_i \nabla C_i) = 0 \tag{4}$$

which provides a single partial differential equation for each component. If the dissociation reactions are fast, we also have J_i algebraic relations among the component i species,

$$K_{ij} = \frac{H_3O^+ S_{ij}}{S_{ij+1}} \tag{5}$$

which must be solved together with Eq. (4) for each component.

Now define the current density, $\vec{I}$, and the charge density, ρ, as

$$\vec{I} = F \sum_{i=1}^{I} (-D_i \nabla (\langle z_i \rangle C_i) + \langle z_i \rangle \vec{U} C_i + \langle z_i^2 \rangle \omega_i \vec{E} C_i) \tag{6}$$

$$\rho = F \sum_{i=1}^{I} \left(\sum_{j=1}^{J_i+1} z_{ij} S_{ij} \right) = F \sum_{i=1}^{I} \langle z_i \rangle C_i \tag{7}$$

where $\langle z_i^2 \rangle C_i = \sum_{j=1}^{J_i+1} z_{ij}^2 S_{ij}$, F is the Faraday constant, and I is the number of components which include H_3O^+ and OH^- ions as $I-1$th and Ith components. For microfluidic applications where the charge density, $\rho \approx 0$, we obtain the electroneutrality constraint as

$$\rho = F \sum_{i=1}^{I} \langle z_i \rangle C_i = 0 \tag{8}$$

3. COMPUTATIONAL MODEL AND ASSUMPTIONS

The set of equations that must be simultaneously solved consists of one conservation Eq. (4) for each component in our system except hydronium (and hydroxyl), an electroneutrality condition of the form,

$$C_{\mathrm{H}} - \frac{K_{\mathrm{W}}}{C_{\mathrm{H}}} = -\sum_{i=1}^{I-2} \langle z_i \rangle C_i \tag{9}$$

which allows us to solve for hydronium (and hydroxyl) ion concentrations and an equation for the electric potential based on the true current, as

$$\nabla \cdot \left[F \sum_{i=1}^{I} \sum_{j=1}^{J_i+1} z_{ij}^2 \omega_{ij} S_{ij} \vec{E} \right] = \sum_{i=1}^{I} \sum_{j=1}^{J_i+1} z_{ij} D_{ij} \nabla \cdot \nabla S_{ij} \tag{10}$$

The concentrations of amphoteric molecules are obtained from the component equations. It is assumed that during IEF, all ionic components, including water, are in chemical equilibrium which implies that the ionic reactions are fast enough that the individual components remain in a pseudo-equilibrium state. In this study, each ampholyte is considered as biprotic, i.e., only the two dissociation constants on either side of their isoelectric points dominate the transient behavior of the carrier ampholytes. Two model proteins, each having ten charge states, are allowed to focus in the microchannel.

This model neglects Joule heating since relatively smaller electric fields are used for separation. Electric field induced electrokinetic flow is not considered here because of the fact that, in our experiments, the IEF channel is generally coated with methylcellulose or other chemicals to suppress electroosmosis.[16, 17] For a given component, the absolute mobilities of all of its charge states are assumed to be the same. The Nernst-Einstein equation ($D_i = (RT\omega_i)/(F)$) is used to calculate the diffusion coefficient from the absolute mobility,[18] where R is the gas constant and T is the absolute temperature.

The concentration of hydronium is calculated from the electroneutrality equation, while the hydroxyl concentration is obtained from the equilibrium relationship ($K_{\mathrm{W}} = C_{\mathrm{OH}} C_{\mathrm{H}}$), where K_{W} is the equilibrium constant for water. The electric potential (ϕ) is calculated from the charge conservation equation using the mean-square valence for all proteins and ampholytes.

The boundary conditions for the mass conservation equations consist of imposition of zero net flux at the anolyte and catholyte reservoirs and on the channel surfaces. The charge conservation equation is solved for insulating boundary conditions ($\nabla\phi \cdot \vec{n} = 0$) on the solid channel surfaces and constant electric potentials at the anolyte and catholyte reservoirs. The insulating boundary condition at the channel wall is justified because silicon, glass, PDMS or some other insulating material is typically used as microchannel substrate.

4. DIFFERENTIAL RESOLUTION

In this section, an analysis is presented for the differential resolution of model proteins in order to compare predictions of the resolution between the analytical solution and the numerical simulation. To do this using data from a single simulated protein peak, we expand the resolution in a Taylor series for vanishingly small differences in the protein pIs and then compare the derivative of the resolution with respect to the pI in the limit as $\Delta pI \to 0$.

Consider a straight microchannel with a linear pH gradient and constant conductivity in which several proteins are focused. The limiting resolution of analytical IEF can be expressed as[19]

$$R_s = \frac{\Delta pI}{4} \sqrt{\frac{FE_x \left| \frac{\partial z}{\partial \mathrm{pH}} \right|}{RT \frac{\partial \mathrm{pH}}{\partial x}}} \approx \left. \frac{\partial R_s}{\partial pI} \right|_{\Delta pI \to 0} \Delta pI \tag{11}$$

where the derivative of the resolution with respect to the isoelectric point is

$$\frac{\partial R_s}{\partial pI} = \frac{1}{4} \sqrt{\frac{FE_x \left| \frac{\partial z}{\partial \mathrm{pH}} \right|}{RT \frac{\partial \mathrm{pH}}{\partial x}}} \tag{12}$$

For a particular protein, constant electric field and fixed pH gradient in the system, the differential resolution is a constant.

On the other hand, one can find the limiting resolution of focused bands from the numerical results using moment analysis

$$R_s = \frac{x_{pI,1} - x_{pI,2}}{2(\sigma_1 + \sigma_2)} \tag{13}$$

where $x_{pI,1}$ and $x_{pI,2}$ are the locations of focal points of two adjacent protein bands, and σ_1 and σ_2 are the standard deviations of the respective bands. In the above expression, if it is assumed that the local pH gradient is constant (not stair-stepped) and proteins are focused in Gaussian form then the standard deviations of both peaks are the same $\sigma_1 = \sigma_2 = \sigma$ and Eq. (13) can be rewritten as

$$R_s = \frac{x_{pI,1} - x_{pI,2}}{4\sigma} \tag{14}$$

and the corresponding differential resolution can be found as

$$\frac{\partial R_s}{\partial pI} = \frac{1}{4\sigma} \left(\frac{\partial x}{\partial pI} \right) = \frac{1}{4\sigma} \left(\frac{x_{pI,1} - x_{pI,2}}{pI_1 - pI_2} \right) = \frac{1}{4\sigma} \left(\frac{\partial x}{\partial \mathrm{pH}} \right) \tag{15}$$

5. NUMERICAL SCHEME

In this work, a 2D finite volume method (2D FVM) is utilized to solve the transport equations with electromigration and diffusion given by Eq. (4) together with the charge conservation equation defined in Eq. (10). Details

RESEARCH ARTICLE

of the numerical scheme are presented in our earlier publication.[15] Briefly, discretized algebraic equations are obtained at each grid point for the mass and charge conservation equations. The power law scheme is used to form coefficients of algebraic equations.[20] The tri-diagonal matrix algorithm (TDMA) is used to solve the discretized algebraic equations along a grid line, and a line by line iteration is employed until conserved results are obtained throughout the computational domain. In the case of the electroneutrality equation, the Newton-Raphson method is used to obtain the concentration of hydronium ions. In our simulation, the convergence criteria are 10^{-4} for mass conservation and 10^{-5} for charge conservation and chemical electroneutrality. Since the mathematical model of IEF is highly nonlinear, structured grids are used for the sake of computational simplicity and stability. In order to obtain grid-independent results, 8000 elements are used (400 grids in the x-direction and 20 grids in the y-direction) for both straight and contraction-expansion microchannels (Fig. 1). The IEF simulation was conducted in 3.4 GHz (CPU) and 4GB (RAM) cluster machines. It took 5 days CPU time to solve each case.

6. RESULTS AND DISCUSSION

In an IEF simulation, one has to simultaneously solve the coupled, non-linear PDEs for all amphoteric components (proteins and ampholytes) in addition to computing the relationships between species and components. This fact makes computer simulations of isoelectric focusing very complicated, memory intensive, and time-consuming. In multidimensional IEF, the most common challenge involves how one treats protein in a discretized fashion on a computer simulation. Unlike low molecular weight ampholytes, proteins consist of a combination of 20 standard amino acids that have carboxyl groups, amino groups and R groups.[21] As a result, proteins will occupy a number of charge states at a given pH range, and they cannot be handled using three charge states only. In this study two model proteins are selected to demonstrate focusing behavior in a multi-dimensional electric field. The pK values of these model proteins are presented in Table I.

In ampholyte-based IEF, the formation of a pH gradient is governed by the factors such as electric potential, diffusion coefficient, mobility, reaction constants of ampholytes and hydronium gradients. It is very difficult to produce the best pH curve in a micro- or nano-fluidic channel, considering all the above factors due to their highly nonlinear relationship. In this work, the effects of ΔpK on IEF are studied in 2D microgeometries, while all other factors are fixed during the simulation process. Two different microgeometries are considered here: a straight microchannel (Fig. 1(a)) and a contraction-expansion microchannel (Fig. 1(b)).

Table I. Electrochemical properties of model proteins used in the IEF simulation. The initial concentration of each protein is 0.016 [mole/m^3] and the absolute mobility of all protein is 3.0E-08 [m^2/Vs].

Reaction constants	Model protein 1 ($pI = 7.46$)	Model protein 2 ($pI = 8.46$)
pK_1	6.20	6.20
pK_2	6.60	6.30
pK_3	7.00	6.80
pK_4	7.25	7.10
pK_5	7.50	7.20
pK_6	8.45	8.20
pK_7	9.40	8.90
pK_8	10.30	9.00
pK_9	11.20	9.40

6.1. Isoelectric Focusing in a Straight Microchannel

For the planar microchannel shown in Figure 1(a), a monotonic pH gradient is simulated using 25 biprotic ampholytes whose physicochemical characteristics are summarized in Table II. Here the ΔpIs of the ampholytes are uniform and two model proteins ($pIs = 7.46$ and 8.46) with ten charge states are allowed to focus in the pH range of 6∼9. The potential at the cathode is set at 0 V (ground), while the potential at the anode is fixed at 300 V. It is assumed that all ampholytes and proteins are uniformly mixed and distributed along the channel at the beginning

Table II. Electrochemical properties of biprotic ampholytes used in the IEF simulation. Six different values of ΔpKs ($\Delta pK = 1$, 1.5, 2, 2.5, 3, and 3.5) are studied here. The initial concentration of each ampholyte is 0.16 [mole/m^3] and the absolute mobility of all ampholyte is 3.0E-08 [m^2/Vs].

Component	pK_1	pK_2	pI
Ampholyte 1	$6.000-0.5\Delta pK$	$6.000+0.5\Delta pK$	6.000
Ampholyte 2	$6.125-0.5\Delta pK$	$6.125+0.5\Delta pK$	6.125
Ampholyte 3	$6.250-0.5\Delta pK$	$6.250+0.5\Delta pK$	6.250
Ampholyte 4	$6.375-0.5\Delta pK$	$6.375+0.5\Delta pK$	6.375
Ampholyte 5	$6.500-0.5\Delta pK$	$6.500+0.5\Delta pK$	6.500
Ampholyte 6	$6.625-0.5\Delta pK$	$6.625+0.5\Delta pK$	6.625
Ampholyte 7	$6.675-0.5\Delta pK$	$6.675+0.5\Delta pK$	6.675
Ampholyte 8	$6.875-0.5\Delta pK$	$6.875+0.5\Delta pK$	6.875
Ampholyte 9	$7.000-0.5\Delta pK$	$7.000+0.5\Delta pK$	7.000
Ampholyte 10	$7.125-0.5\Delta pK$	$7.125+0.5\Delta pK$	7.125
Ampholyte 11	$7.250-0.5\Delta pK$	$7.250+0.5\Delta pK$	7.250
Ampholyte 12	$7.375-0.5\Delta pK$	$7.375+0.5\Delta pK$	7.375
Ampholyte 13	$7.500-0.5\Delta pK$	$7.500+0.5\Delta pK$	7.500
Ampholyte 14	$7.625-0.5\Delta pK$	$7.625+0.5\Delta pK$	7.625
Ampholyte 15	$7.675-0.5\Delta pK$	$7.675+0.5\Delta pK$	7.675
Ampholyte 16	$7.875-0.5\Delta pK$	$7.875+0.5\Delta pK$	7.875
Ampholyte 17	$8.000-0.5\Delta pK$	$8.000+0.5\Delta pK$	8.000
Ampholyte 18	$8.125-0.5\Delta pK$	$8.125+0.5\Delta pK$	8.125
Ampholyte 19	$8.250-0.5\Delta pK$	$8.250+0.5\Delta pK$	8.250
Ampholyte 20	$8.375-0.5\Delta pK$	$8.375+0.5\Delta pK$	8.375
Ampholyte 21	$8.500-0.5\Delta pK$	$8.500+0.5\Delta pK$	8.500
Ampholyte 22	$8.625-0.5\Delta pK$	$8.625+0.5\Delta pK$	8.625
Ampholyte 23	$8.675-0.5\Delta pK$	$8.675+0.5\Delta pK$	8.675
Ampholyte 24	$8.875-0.5\Delta pK$	$8.875+0.5\Delta pK$	8.875
Ampholyte 25	$9.000-0.5\Delta pK$	$9.000+0.5\Delta pK$	9.000

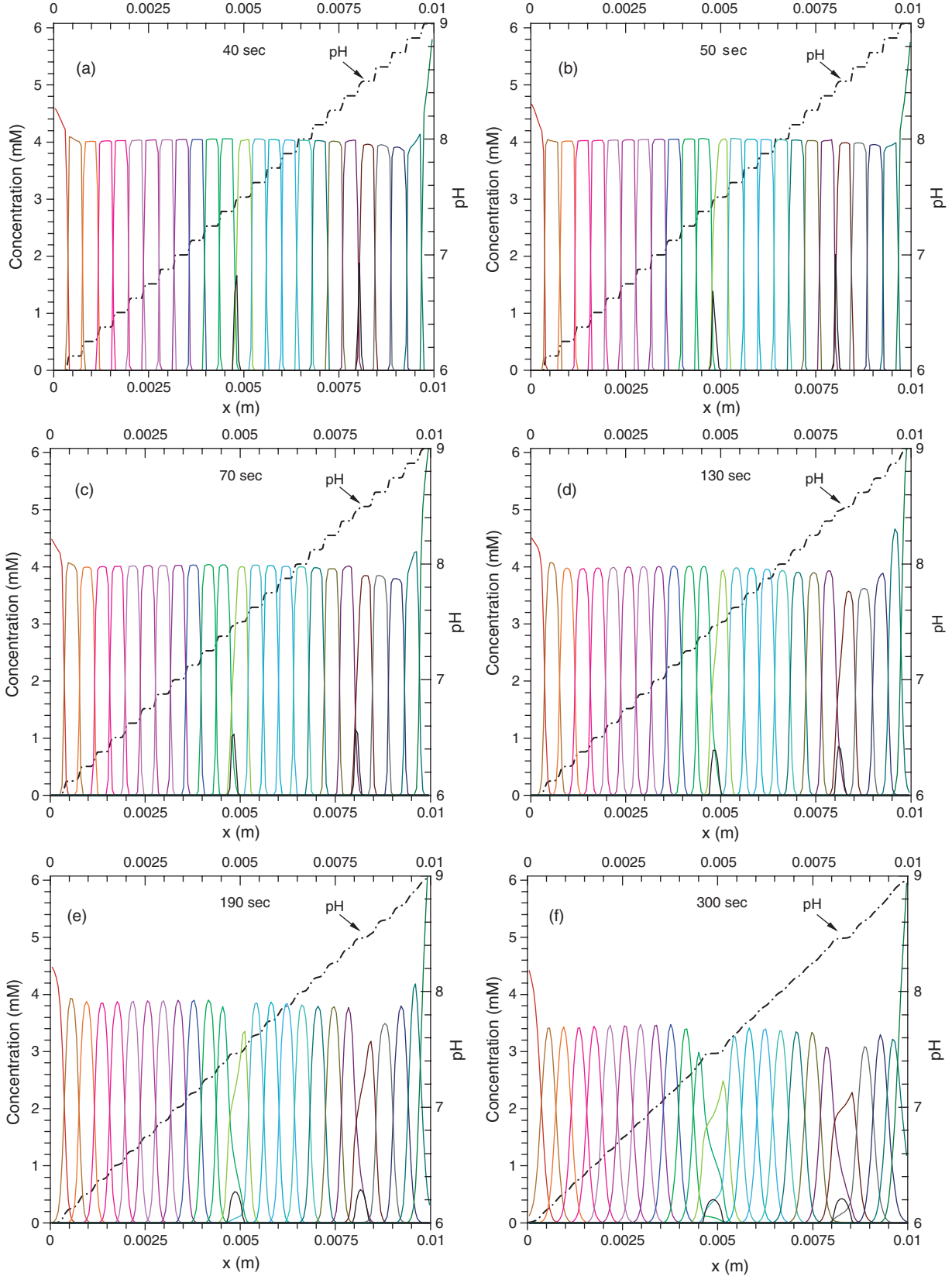

Fig. 2. Steady state concentration distribution for ampholytes and proteins in a straight microchannel. (a) $\Delta pK = 1$, (b) $\Delta pK = 1.5$, (c) $\Delta pK = 2$, (d) $\Delta pK = 2.5$, (e) $\Delta pK = 3$, and (f) $\Delta pK = 3.5$. Numerical results are extracted along the channel center line $(A - A')$ of Figure 1(a).

of the separation process. The initial concentration of each ampholyte is 10 times higher than that of the protein and all ampholytes are treated as having 3 charge states.

The steady state concentration profiles of ampholytes and proteins in a straight microchannel are shown in Figure 2 for different values of the ΔpK. Numerical results show that the concentration profiles of focused ampholytes depend on the ΔpK. For instance, a Gaussian distribution is obtained for $\Delta pK > 3$, while rectangular shape results for $\Delta pK < 3$. The effect of ΔpK on ampholyte concentration can be explained from the pH and net charge (z) distribution. Figure 3 shows the titration curve of ampholytes #13 (Table II) for different values of the ΔpK. A similar trend will be obtained for other ampholytes, except that their pIs (zero charge) will be shifted. From Figure 3 it is clear that the titration curve (charge variations) of a biprotic ampholyte is very steep at its pI point for lower values of ΔpK. In other words, near the pI, a small change in pH will result in a large variation in net charge for an ampholyte. This fact contributes to clustering of a particular ampholyte at its pI so a rectangular concentration profile is formed. Here the bandwidth and peak height of ampholytes depend on the number of ampholytes and initial molar concentration of ampholytes. On the other hand, for large ΔpK the titration curve is very flat allowing the charge to remain almost constant over a wide range of pH, and a Gaussian type distribution is expected. For $\Delta pK = 3.5$, all ampholytes occupy nearly equal volumes of the 2D channel at nearly identical Gaussian concentrations with the exception of ampholytes 12, 13 and 21 close to the two proteins. The main reason for this that the broad peak width of model proteins displaces the neighboring ampholyte sufficiently to reduce their height.

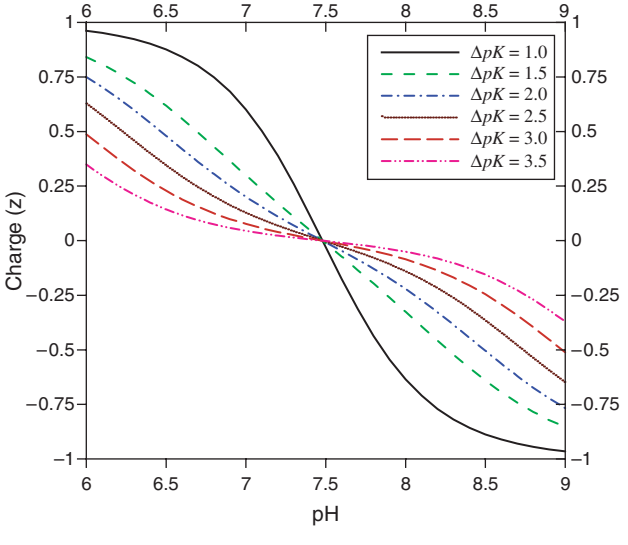

Fig. 3. Titration curves of ampholyte #13 ($pI = 7.50$) at different ΔpKs. For smaller values of ΔpK, the charge gradient is very steep at isoelectric points, which helps in forming rectangular shape tight focused bands of ampholytes.

The simulation data also reveals that the peak concentration of the focused protein depends on the value of ΔpK (Fig. 2). At steady state, the peak concentrations of protein 1 ($pI = 7.46$) are 1.66, 1.50, 1.03, 0.79, 0.55 and 0.41 mM corresponding to the $\Delta pK = 1$, 1.5, 2, 2.5, 3 and 3.5. In other words, the peak width of proteins increases with ΔpK. Similar trends are also observed for the second protein for which pI is 8.46. The peak heights of second protein are 1.88, 1.65, 1.15, 0.85, 0.59, 0.43 mM for $\Delta pK = 1$, 1.5, 2, 2.5, 3 and 3.5, respectively. Simulation results also demonstrate that, for both proteins, the peak concentration decreases abruptly when ΔpK is changed from 1.5 to 2. This is due to the change in ampholytes' shape closest to the focused protein(s). From Figures 2(b and c) it is clear that the shape of ampholytes #12 and 13 changes from rectangular at $\Delta pK = 1.5$ to Gaussian at $\Delta pK = 2.0$. A similar transition in shape is also evident for ampholyte #20 and 21 when ΔpK is increased from 1.5 to 2.0.

To study the effect of ampholyte dissociation constants on pH profile, the steady state pH distribution is also presented in Figure 2. It is important to note that linear-like pH curves are being approached with the increase of ΔpK, but the linear pH curve is not obtained until $\Delta pK = 3.5$. As a matter of fact, it is reported that a stepwise pH profile is formed if a small number of ampholytes are used in the IEF simulation.[6, 15] In the past some researchers studied the conditions for avoiding the stepwise pH phenomenon.[22, 23] Through an analytical work, Svensson proposed that the nearest distance of two ampholytes (ΔpI) should be less than three standard deviations (σ) for a stepless pH profile.[22] Based on numerical results, Mosher et al. modified the condition (or criterion) to form a linear pH profile for ampholyte-based IEF in 1D geometry.[6] According to them, stepless pH profile can be obtained if $\Delta pI < 2\sigma$. In this paper, the required ΔpI of ampholytes is calculated for linear pH production by varying the difference in two dissociation constants (ΔpK), while all other conditions are held constant ($E_x = 300$ V/cm, $\Delta\text{pH} = 6 \sim 9$, $\omega = 3.0\text{E-}8$ m^2/Vs). Our numerical results show that, for 25 biprotic ampholytes, the linear pH profile cannot be obtained until $\Delta pK < 3$. This suggests that a more restrict condition ($\Delta pI < \sigma$) is needed for linear pH profile. It is important to note that a constant electric potential is applied in our simulation, while constant electric current density is used in other studies. Nevertheless, the ΔpK of ampholytes has a direct impact on the formation of pH gradient in the system. Simulation results also show that, for a fixed number of ampholytes, a stair-stepped pH gradient gives a better result than a smooth gradient.

6.2. Isoelectric Focusing in a Contraction-Expansion Microchannel

To examine the pH formation and focusing behavior of proteins in complex microgeometries, a 3:1:3 gradual

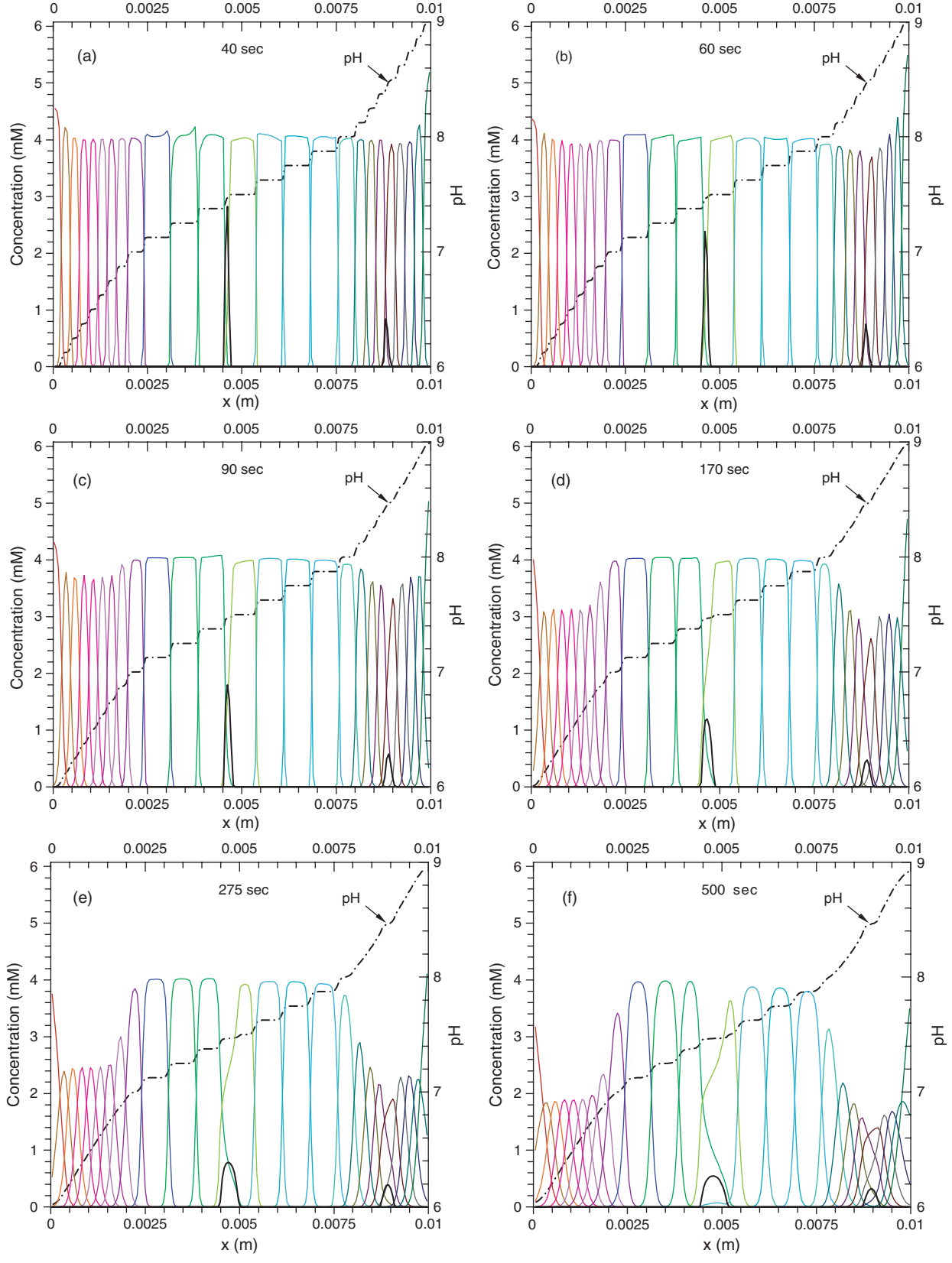

Fig. 4. Steady state concentration distribution for ampholytes and proteins in a contraction-expansion microchannel. (a) $\Delta pK = 1$, (b) $\Delta pK = 1.5$, (c) $\Delta pK = 2$, (d) $\Delta pK = 2.5$, (e) $\Delta pK = 3$, and (f) $\Delta pK = 3.5$. Numerical results are extracted along the channel center line ($A - A'$) of Figure 1(b).

contraction-expansion channel is selected as depicted in Figure 1(b). Like the straight channel (Fig. 1(a)), the pH gradient is formed in the presence of the 25 biprotic ampholytes presented in Table II, while two model proteins with 10 charge states (Table I) are allowed to focus within a pH range of 6–9. Here the channel width on the anodic side before the contraction region and the cathodic side after the expansion region is 1.5 mm, the width of the throat region is 0.5 mm, and the total channel length is 1 cm. The oblique angles connecting the expanded and contracted sections are set at 30°. For the contraction-expansion channel, all input parameters, initial and boundary conditions for ampholytes and proteins are identical with those of the straight channel.

Figure 4 presents the concentration distributions of proteins and ampholytes in a 3:1:3 contraction-expansion channel at steady state for different cases ($\Delta pK = 1, 1.5, 2, 2.5, 3, 3.5$). The main feature of IEF simulation in a contraction-expansion channel is the geometric effect on the ampholytes and proteins. In Figure 4, the ampholytes in the contracted throat region ($0.25 < x < 0.75$ cm) have focused to broad, rectangular bands and the ampholytes in the two expanded regions are focused into narrower, Gaussian bands. This is due to the fact that the throat region has a smaller cross section, and those ampholytes that focus in this section must occupy a greater length of the channel resulting in a so-called "Zoom" effect. This "Zoom" effect cannot be found in a straight channel and a 1D model cannot be used to simulate it. This "Zoom" effect also contributes to the shallow pH gradient in the throat region. Figure 4 shows that the protein ($pI = 7.46$) in the throat region is more tightly focused than the protein ($pI = 8.46$) in the expansion region ($0.75 \leq x \leq 1$ cm). The higher peak concentration of the protein in the throat region is primarily due to the higher (three times) electric field compared with that in the expanded region.

In a contraction-expansion channel, the effect of ΔpK on the pH profile is different from that of a straight microchannel. For instance, a linear pH profile is obtained in the expanded region ($0. \leq x \leq 0.25$ cm) for $\Delta pK \geq 2$ due to presence of more ampholytes than in the straight channel case. On the other hand, the pH profile is step-wise in the throat region for the parametric range (ampholyte ΔpK) studied here. In other words, the pH formation varies with channel shape. The numerical results show that the ratio of peak heights between the protein in the throat region and the protein in the expansion region decreases with ΔpK. The peak height ratios are obtained as 3.3, 3.3, 3.0, 2.7, 2, and 1.74 for $\Delta pK = 1, 1.5, 2, 2.5, 3,$ and 3.5, respectively. That means the smaller ΔpKs give a tighter peak due to the steeper titration curve.

6.3. Focusing Time and Resolution

Figure 5 shows the effect of ΔpK on the initial focusing time of the proteins. In this paper, the initial focusing time is defined as the time that the pair of protein peaks (so called double peaks) that initially form from a single component at the opposite ends of the channel takes to coalesce into a single band. Numerical results show that the initial focusing time (aka merging time) increases with ΔpK. In a straight channel, the initial focusing times for protein 1 are 10, 11, 13, 17, 21, and 27 sec and the focusing times to reach the steady state are 40, 50, 70, 150, 190, and 300 sec corresponding to the $\Delta pK = 1, 1.5, 2, 2.5, 3$ and 3.5. These times are related to the charge gradient of the ampholytes, which varies with ΔpK. At low ΔpK, the charge gradient is very sharp causing less time for the ampholytes to focus in the channel. Once the ampholytes are focused, the double peaks of proteins continue to move toward their pI points until they reach steady profiles.

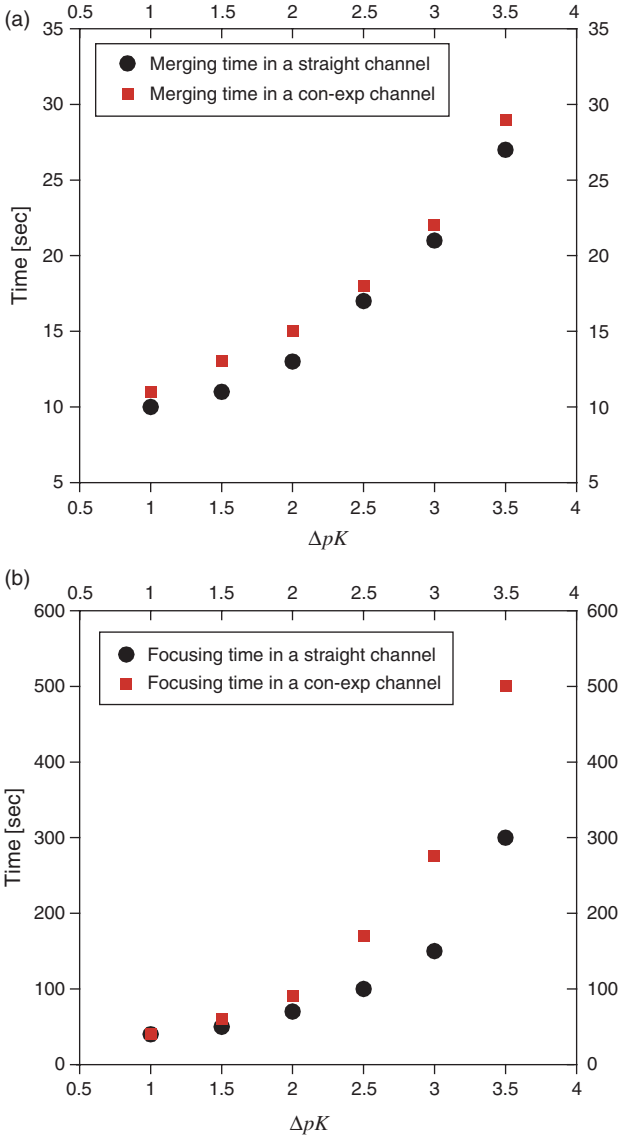

Fig. 5. Comparison of (a) merging time and (b) focusing time for straight and contraction-expansion microchannels.

Like the straight channel case, the focusing times of protein 1 ($pI = 7.46$) also increase with ΔpK for contraction-expansion channel as shown in Figure 5. However, both merging and focusing times are higher for the contraction-expansion channel than those of a straight channel. This phenomenon is consistent with the experimental observation where longer period is required if a complex microgeometry is used to focus proteins instead of straight channel.[17] For a particular ΔpK, a longer time is required to form a stable pH profile in contraction-expansion channel due to the nonlinear interaction among channel geometry, electric field and ampholytes.

The differential resolutions of the focused proteins are presented in Figure 6 for both straight and contraction-expansion microchannels. In this study, protein 1 ($pI = 7.46$) is considered for differential resolution calculation. At the mid section ($0.25 < x < 0.75$ cm), the electric field and pH gradient are different in straight and contraction-expansion microchannels due to the different channel width. As expected, the theoretical value of the differential resolution remains constant for both straight and contraction-expansion microchannel since the ΔpKs of the ampholytes are not considered in the simple linear model. However, our nonlinear numerical results show that the differential resolution decreases with the increase in ΔpK. In other words, the resolution of focused bands will be higher at low ΔpK values. Moreover, the "Zoom" region of the contraction-expansion channel can resolve proteins with higher efficiency.

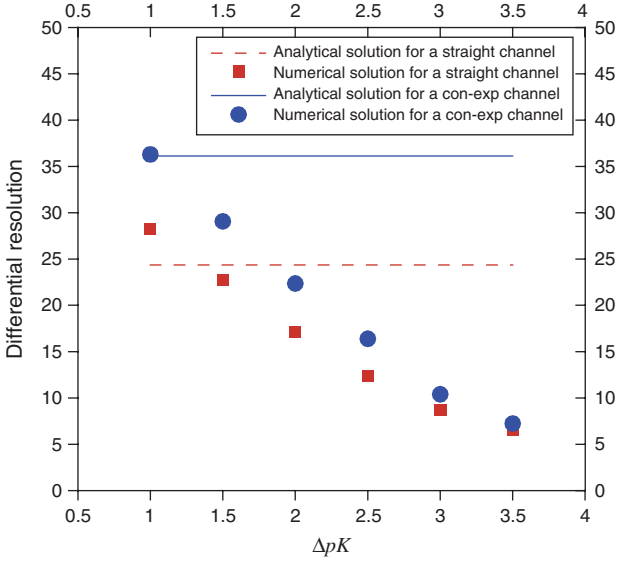

Fig. 6. Differential resolution of focused proteins in straight and contraction-expansion microchannels. Eqs. (12) and (15) are used to calculate theoretical and numerical differential resolution, respectively. The numerical differential resolution decreases with increasing ΔpK, while the analytical differential resolution remains constant for a particular protein.

7. CONCLUSIONS

The effects of varying the ampholyte dissociation constants are investigated for isoelectric focusing in 2D straight and contraction-expansion microchannels. A finite-volume based numerical technique is developed to solve mass conservation of ampholytes and proteins, charge conservation, and electroneutrality equations. Two model proteins are focused in the presence of 25 biprotic ampholytes under constant electric potentials at the electrode reservoirs. Six different ΔpK values are considered for the biprotic ampholytes, while each protein is modeled as having ten charge states.

In a 2D straight microchannel, for low ΔpK ($\Delta pK < 2$), each ampholyte focuses at its respective pI with a rectangular distribution. The model proteins behave in a fashion similar to the ampholytes except that, since the initial number of moles of protein is substantially smaller than that of the ampholytes, they focus to a near-Gaussian peak rather than to a plateau. However, at higher values of ΔpK ($\Delta pK > 2$), each ampholyte forms a Gaussian distribution around its pI value. The simulation data show that, for 25 ampholytes, a linear pH profile, $6 < \text{pH} < 9$, exists between $\Delta pK = 3.0$ and $\Delta pK = 3.5$ in a 1 cm long straight channel for a nominal electric field of 300 V/cm.

For a contraction-expansion microchannel, a stepwise pH curve is formed in the throat region for ΔpK between 1 and 3.5, while a smooth pH curve is obtained in the expanded regions for $\Delta pK \geq 2$. Moreover, in a contraction-expansion microchannel, a protein is more finely resolved in the throat region than in the expanded region due to the higher electric field.

The peak height and differential resolution of proteins decreases with increasing ΔpK for both the straight and contraction-expansion channel. Numerical results show that the merging and focusing time increase with ΔpK for both straight and contraction-expansion microchannels. For a particular ΔpK, the focusing time is longer in the contraction-expansion channel than in a straight channel because of the geometric complexity.

Acknowledgments: This work was supported by the National Science Foundation under Grant No. CTS0300802.

References and Notes

1. H. Svensson, *Acta Chem. Scand.* 15, 325 **(1961)**.
2. H. Svensson, *Biophys.* 1, 131 **(1962)**.
3. J. C. Giddings and K. Dahlgren, *Separ. Sci.* 6, 345 **(1971)**.
4. W. Thormann, T. Huang, J. Pawliszyn, and R. A. Mosher, *Electrophoresis* 25, 324 **(2004)**.
5. Q. Mao, J. Pawliszyn, and W. Thormann, *Anal. Chem.* 72, 5493 **(2000)**.
6. R. A. Mosher, D. A. Saville, and W. Thormann, The Dynamics of Electrophoresis, VCH, Weinheim **(1992)**.
7. I. L. Arnaud, J. Josserand, J. S. Rossier, and H. H. Girault, *Electrophoresis* 23, 3253 **(2002)**.

RESEARCH ARTICLE

8. S. J. Luner and A. Kolin, *Proceedings of the National Academy of Science* 66, 898 **(1970)**.
9. H. Rilbe, *N. Y. Ann. Acad. Sci.* 209, 11 **(1973)**.
10. Q. A. Palusinski, T. T. Allgyer, R. A. Mosher, and M. Bier, *Biophysical Chem.* 13, 193 **(1981)**.
11. M. Bier, Q. A. Palusinski, R. A. Mosher, and D. A. Saville, *Science* 219, 2181 **(1983)**.
12. M. Jaros, K. Vcelakova, I. Zuskova, and B. Gas, *Electrophoresis* 23, 2667 **(2002)**.
13. V. Hruska, M. Jaros, and B. Gas, *Electrophoresis* 27, 984 **(2006)**.
14. L. Onsager and R. M. Fuoss, *J. Phys. Chem.* 36, 2689 **(1932)**.
15. J. Shim, P. Dutta, and C. F. Ivory, *Electrophoresis* 28, 572 **(2007)**.
16. H. Cui, K. Horiuchi, P. Dutta, and C. F. Ivory, *Anal. Chem.* 77, 1303 **(2005)**.
17. H. Cui, K. Horiuchi, P. Dutta, and C. F. Ivory, *Anal. Chem.* 77, 7878 **(2005)**.
18. D. A. Saville and Q. A. Palusinski, *AIChE J.* 32, 207 **(1986)**.
19. P. G. Righetti, Isoelectric Focusing: Theory, Methodology and Applications, Elsevier Biomedical Press, Amsterdam **(1983)**.
20. S. V. Partankar, Numerical Heat Transfer and Fluid Flow, Hemisphere, New York **(1980)**.
21. Lehninger, Principles of Biochemistry, Worth, New York **(1995)**.
22. H. Svensson, *J. Chromatogr.* 25, 266 **(1966)**.
23. M. Almgren, *Chemica Scripta.* 1, 69 **(1971)**.

Received: 3 January 2007. Accepted: 12 May 2007.